



HAL
open science

Catalytic Reduction of Oxygen by a Copper Thiosemicarbazone Complex

Tatiana Straistari, Adina Moroza, Sergiu Shova, Marius Réglie, Maylis Orio,
Vincent Artero

► **To cite this version:**

Tatiana Straistari, Adina Moroza, Sergiu Shova, Marius Réglie, Maylis Orio, et al.. Catalytic Reduction of Oxygen by a Copper Thiosemicarbazone Complex. *European Journal of Inorganic Chemistry*, 2020, 2020 (48), pp.4549-4555. 10.1002/ejic.202000869 . hal-03179025v1

HAL Id: hal-03179025

<https://hal.science/hal-03179025v1>

Submitted on 24 Mar 2021 (v1), last revised 10 May 2021 (v2)

HAL is a multi-disciplinary open access archive for the deposit and dissemination of scientific research documents, whether they are published or not. The documents may come from teaching and research institutions in France or abroad, or from public or private research centers.

L'archive ouverte pluridisciplinaire **HAL**, est destinée au dépôt et à la diffusion de documents scientifiques de niveau recherche, publiés ou non, émanant des établissements d'enseignement et de recherche français ou étrangers, des laboratoires publics ou privés.

Catalytic reduction of oxygen by a copper thiosemicarbazone complex

Tatiana Straistari,^[a,b,c] Adina Morozan,^{*[a]} Sergiu Shova,^[d] Marius Réglier,^[b] Maylis Orio^{*[b]} and Vincent Artero^[a]

- [a] Dr. T. Straistari, Dr. A. Morozan*, Dr. V. Artero
Laboratoire de Chimie et Biologie des Métaux
Université Grenoble Alpes, CNRS, CEA/IRIG
17 rue des Martyrs, F-38054 Grenoble cedex 9, France
E-mail: adina.morozan@cea.fr
- [b] Dr. T. Straistari, Dr. M. Réglier, Dr. M. Orio*
Aix-Marseille Univ., CNRS, Centrale Marseille, iSm2
Marseille, France
E-mail: maylis.orio@univ-amu.fr
- [c] Dr. T. Straistari
Institute of Chemistry
Academy of Sciences of Moldova
3, Academiei street, Chisinau MD 2028, Republic of Moldova
- [d] Dr. S. Shova
Institute of Macromolecular Chemistry "Petru Poni"
41A Grigore Ghica Voda Alley, Iasi 700487, Romania

Supporting information for this article is given via a link at the end of the document.

Abstract: The new copper(II) thiosemicarbazone complex **CuL** ($H_2L = 4$ -bis(4-(*p*-methoxyphenyl)-thiosemicarbazone))-2,3-butane) was synthesized and structurally characterized. Its electrochemical behavior in *N,N*-dimethylformamide (DMF) was examined. This complex proved active for homogeneous oxygen reduction reaction (ORR) in DMF in the presence of organic acids. The activity and selectivity for ORR was found to be dependent on the nature of the proton source (phenol or acetic acid). This study both confirmed the previously reported free energy linear correlation between selectivity and overpotential requirement [Passard et al., *J. Am. Chem. Soc.* 2016, 138, 2925-2928] and suggests that additional descriptors are required for a full understanding of the catalytic ORR behavior.

Introduction

The oxygen reduction reaction (ORR) is a main reaction in energy production, in biological^[1] as well in technological (e.g., fuel cells) processes.^[2] The most desirable catalytic pathway for the ORR is the direct one to water via a $4e^-/4H^+$ process. The undesirable production of reactive oxygen intermediates is the key limiting issue for the biological systems^[3] and for the fuel cell power output.^[2]

In Nature, the enzymatic ORR is known to occur at competitive overpotentials.^[4] Two groups of Cu-based enzymes exhibit good performances as catalysts for the selective reduction process of oxygen to water: (i) cytochrome *c* oxidases (CcOs) exhibit a bimetallic active site consisting of an iron porphyrin heme *a*3 and a tris-histidine-coordinated Cu (Fe_{a3}/Cu_B);^[4-5] (ii) multicopper oxidases (MCOs) such as laccase and bilirubin oxidase, contain at least one mono-nuclear site containing one type-1 (T1) Cu^I or blue copper, a trinuclear site containing one type-2 (T2) Cu^I or normal copper, and two type-3 (T3) Cu^I or coupled binuclear copper.^[6-7] These active sites are inspirations for the design of alternative copper-based catalytic systems towards a complete understating of favorable conditions for a selective ORR to

water. Molecular complexes have generally shown a significant role in the catalysis field in general, and for the ORR in particular, owing to their various advantages such as precise synthetic control, clearly identifiable structure and active sites, tenability or intrinsic activity.^[8-11]

Iron or cobalt complexes are among the most common and widely studied homogeneous ORR catalysts^[12-15] since the discovery of the catalytic nature of cobalt phthalocyanine by Jasinski and co-workers.^[16] The field has matured and many issues have been wholly or partly answered with a series of Co- and Fe-based molecular catalysts, including: (i). standard reduction potentials for O₂ reduction in organic solvents^[17-18], (ii). correlation of the catalytic reaction rate with the overpotential requirement for ORR^[13] and (iii). correlation of the ORR selectivity with metal ion redox potential and standard potential of O₂ reduction.^[15, 18]

Regarding copper complexes, studies on various synthetic coordination complexes inspired by the Cu-based enzymes^[19-22] have helped to clarify some fundamental mechanistic aspects of the oxygen reduction. Such studies provide understanding into the role of the metal environment toward the design of mono- and binuclear copper systems. A number of copper-based molecular structures have already been reported for proton-assisted catalytic reduction of oxygen in the field of sustainable energy conversion.^[23-27] However, these studies were mostly performed using molecular catalysts immobilized onto electrodes surfaces. So that, relatively limited electrochemical information is available for homogeneous ORR catalysis mediated by Cu complexes.^[20-21] In 2010, the first mononuclear copper(II) complex for homogeneous ORR was reported but the assay used a ferrocene derivative as chemical reductant.^[28] Further study of other mononuclear^[29-30] or binuclear^[31-32] copper molecular catalysts for homogeneous ORR catalysis provided insights into electro-assisted ORR catalysis but such examples are still rare.

Thiosemicarbazone are redox active ligands^[33] and are obtained by simple and scalable synthesis approaches. Their structure

can be easily modified to explore different behaviors of metal complexes (stability, redox potential, etc.). We recently demonstrated that Co and Ni complexes of thiosemicarbazone ligands are active as electrocatalysts for the hydrogen evolution reaction.^[33-34]

We describe here the synthesis and characterization of a new copper(II) thiosemicarbazone complex (CuL, Scheme 1) and report on its homogeneous ORR catalytic activity in N,N-dimethylformamide (DMF) in the presence of various acids of different strength (phenol – PhOH, acetic acid – AcOH and trifluoroacetic acid – TFA) used as proton source.

Results and Discussion

Synthesis and characterization

The red copper(II) thiosemicarbazone complex CuL (Figure 1) was obtained from the reaction of 4-(bis(4-(*p*-methoxyphenyl)-thiosemicarbazone))-2,3-butane (H₂L^[33]) and copper(II) nitrate in methanol with a yield of 70 %. Complexation of the L²⁻ ligand is indicated in the IR spectrum by a shift of the $\nu_{C=N}$ band from 1593 cm⁻¹ in H₂L^[33] to 1598 cm⁻¹ in CuL. In addition, thione-thiol tautomerism^[35-36] follows complexation as indicated by the disappearance of the $\nu_{C=S}$ band at 829 cm⁻¹ which is replaced by a new ν_{C-S} band at 821 cm⁻¹ in the spectra of CuL complex.^[33]

The crystal structure (Figure 1) reveals that the ligand adopts an *s-cis* (synperiplanar) conformation of the substituents within the butane unit upon complexation. The Cu ion is four-coordinate and sits by 0.039 Å out of N₂S₂ plane. The three five-membered chelate rings Cu1N3C9C11N4, Cu1N3N2C8S1 and Cu1N4N5C13S2 are also essentially planar with mean plane deviation of Cu coordination center of 0.006(2), 0.027(1) and 0.036(1) Å, respectively. The angles between the coordinate plane and the two phenyl rings C2C3C4C5C6C7 and C14C15C16C17C18C19 are of 27.1(1)° and 4.8(1)°, respectively.

The ligand is in the thiolate form which is evidenced by the increase of the C1-S8 and C13-S2 bond distances (1.762(4) Å and 1.751(5) Å, respectively) compared to those observed for the neutral ligand H₂L (1.674 Å and 1.673 Å, respectively).^[33]

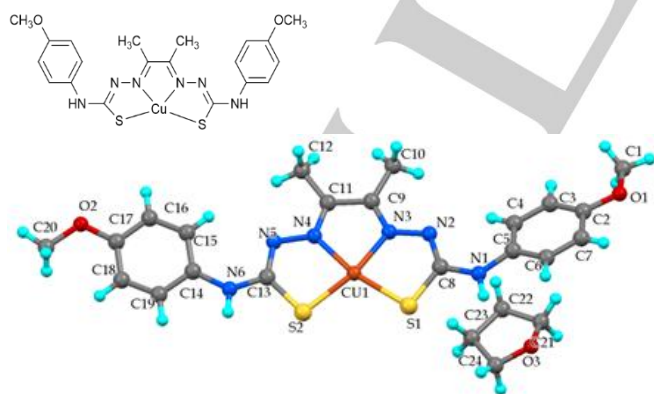


Figure 1. Molecular and X-ray crystal structures of [CuL]·THF with atom labelling scheme and ellipsoids parameters at 50 % probability level. Selected bond lengths: Cu(1)–S(1) 2.2170(14) Å, Cu(1)–S(2) 2.2145(12) Å, Cu(1)–N(3) 1.950(3) Å, Cu(1)–N(4) 1.944(4) Å. Selected bond angles: S(2)–Cu(1)–S(1) 107.77(5)°, N(3)–Cu(1)–S(1) 85.91(13)°, N(3)–Cu(1)–S(2) 165.70(13)°, N(4)–Cu(1)–S(1) 167.09(10)°, N(4)–Cu(1)–S(2) 85.07(10)° and N(4)–Cu(1)–N(3) 81.19(15)°.

Electronic absorption spectrum recorded in DMF for the CuL neutral complex exhibits two intense bands at $\lambda_{max} = 405$ and 485 nm (Figure 2b, black line).

Electrochemical characterization

The cyclic voltammograms of CuL complex (Figure 2a and Figure S1-a) recorded in DMF over the potential range from –1.5 V to 0.7 V vs NHE exhibit only one electrochemically reversible process observed at $E_{1/2} = -0.48$ V vs NHE (where $E_{1/2} = [E_{pc} + E_{pa}]/2$) corresponding to the Cu^{II}/Cu^I redox couple. The peak current (i_p) varies linearly with the square root of the scan rate ($\nu^{1/2}$), indicating a diffusion-controlled process (Figure S1-b). Spectro-electrochemical measurements performed at –0.65 V vs NHE show a uniform decrease of the absorption profile (bands at 405 and 485 nm) with the concomitant formation of a new absorption band at 361 nm ($\epsilon \times 10^{-4} = 2.42$ L·mol⁻¹·cm⁻¹) when CuL is reduced. The reduction process proceeds smoothly with an isosbestic point at 396 nm. Reoxidation at –0.20 V vs NHE leads to an UV-vis spectrum (Figure 2b, red line) similar to the initial one (Figure 2b, black line and Table S1), confirming the full reversibility of the one-electron electrochemical process observed at –0.48 V vs NHE.

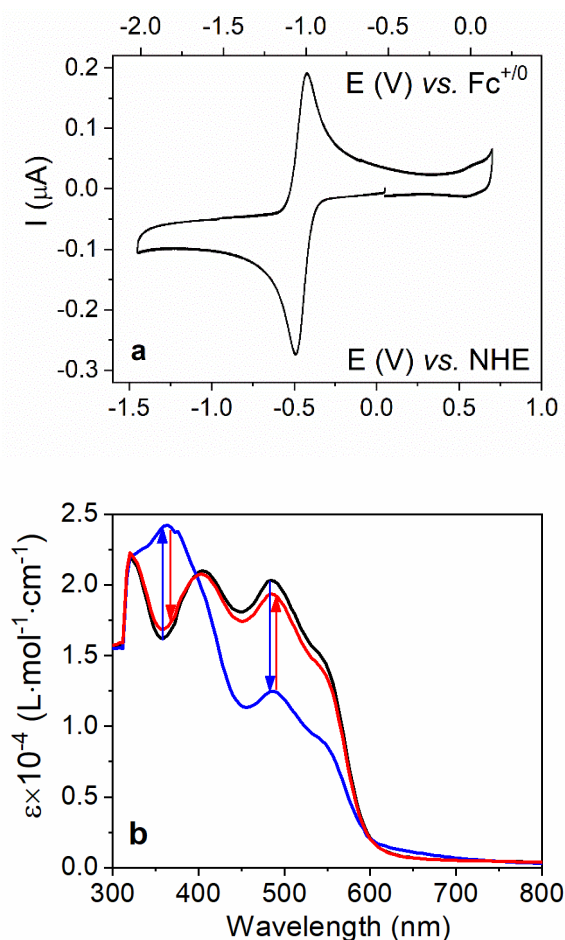


Figure 2. a). Cyclic voltammogram of CuL (1 mM) recorded under Ar-saturated DMF (0.1 M ^tBu₄NPF₆), on GC electrode (ø 1.6 mm), scan rate 100 mV·s⁻¹; b). Electronic absorption spectra for the neutral CuL (0.35 mM, black line), one-electron-reduced species CuL⁻ (blue line) and electrochemically reoxidized CuL (red line).

Theoretical calculations

In an effort to understand the redox behavior of **CuL**, DFT calculations were undertaken and the structure of the complex was subjected to geometry optimization. DFT calculations show that the Cu–S and Cu–N bond lengths for the computed structure are comparable to those determined by X-ray crystallography which confirms the presence of a Cu^{II} center in **CuL** ([Cu^{II}L]⁰, S = ½, Table S2 and Figure S2). Geometry optimization was also conducted on the one-electron reduced **CuL**[−] species. The resulting structure shows an elongation of both the Cu–N and Cu–S bond lengths consistently with a metal-based reduction process and the formation of a Cu(I) diamagnetic species ([Cu^IL][−], S = 0). These theoretical results support that the observed redox process is assigned to the Cu^{II}/Cu^I couple.

The DFT-calculated electronic structure of **CuL** leads to a Single Occupied Molecular Orbital (SOMO) for the neutral species that is mainly distributed on the metal center (44 %) with non-negligible contributions from the coordinating atoms (30 %, S-

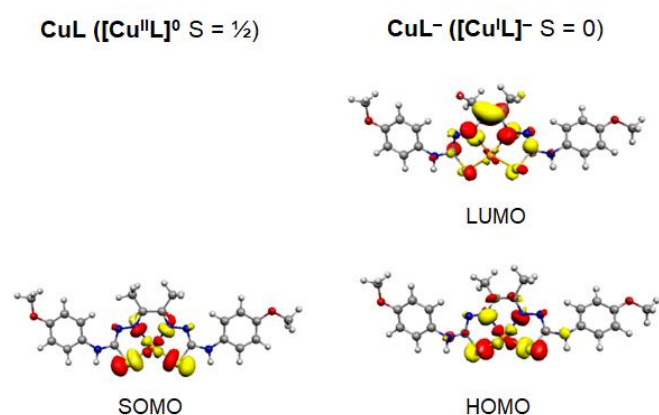


Figure 3. DFT-calculated redox-active orbitals for **CuL** and **CuL**[−].

atoms and 25 %, N-atoms) which is typical for a mononuclear Cu^{II} complex in a square planar geometry (Figure S3). In the one-electron reduced species, the Highest Occupied Molecular Orbital (HOMO) is also distributed over the metal and the first coordination sphere, which is the proof of a metal-centred reduction process (Figure 3). Redox potential calculations were also conducted to assign the electrochemical event in **CuL** (Table S3). The computed values for the one-electron reduction process leading to **CuL**[−] is of −0.55 vs NHE. The computed potential value is in fair agreement with the experimental data and thus support the assignment of the reduction loci in the complex.

Catalytic O₂ reduction activity

The cyclic voltammogram of **CuL** (black traces, Figures 4, a-c) was significantly modified when O₂ is bubbled into the DMF solution (blue traces, Figure 4, a-c): A slight increase in the cathodic current is observed while the backward anodic peak is disappeared. This behavior indicates that the **CuL** complex react with O₂ following one-electron reduction of the copper core.

Addition of phenol (PhOH, pK_a = 1.8)^[37] or acetic acid (AcOH, pK_a = 13.3)^[38] to the O₂-saturated solutions triggers the appearance of catalytic waves with half-wave potentials similar to that of the Cu^{II}/Cu^I couple (Figures 4, a and b). Such a catalytic wave likely corresponds to ORR and was not observed in the absence of the **CuL** complex (Figure 4, a and b, dashed curves). The catalytic response depends on the strength and the concentration (Figure

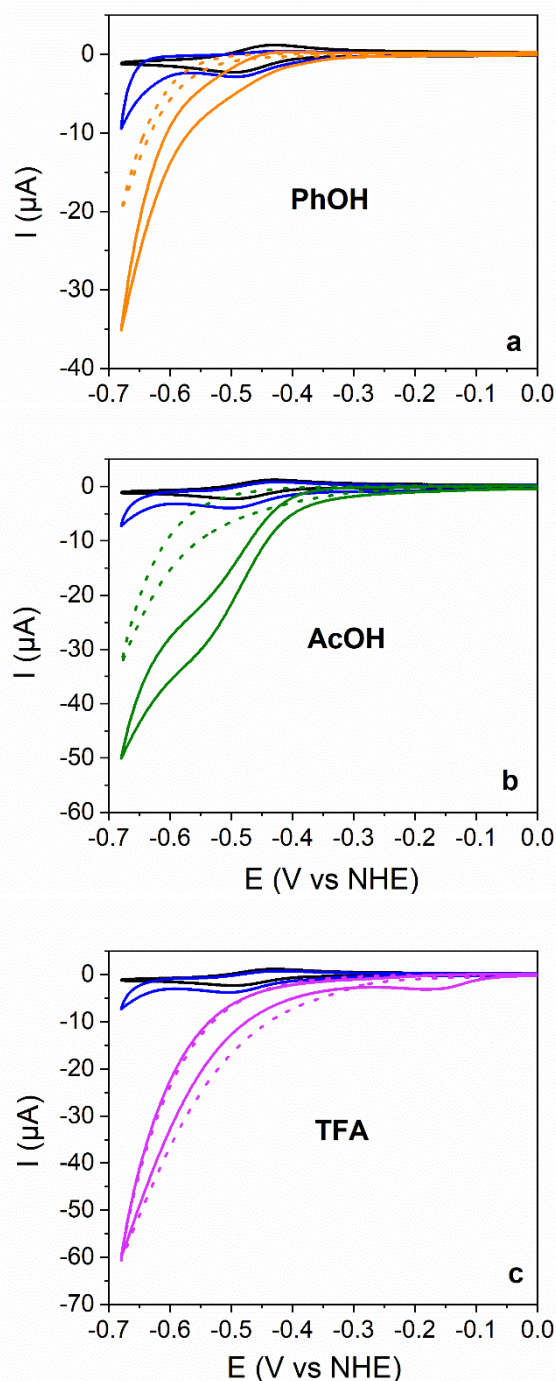


Figure 4. Cyclic voltammograms for **CuL** (1 mM) in DMF (0.1 M nBu₄NPF₆) on GC electrode (ø 5 mm), scan rate 100 mV·s^{−1}, under Ar-saturated atmosphere (black curves), O₂-saturated atmosphere (blue curves) and O₂-saturated atmosphere with the addition of: a. PhOH (50 mM, orange curves), b. AcOH (50 mM, green curves), c. TFA (50 mM, purple curves). The CVs of acids recorded under O₂-saturated atmosphere in the absence of **CuL** are shown in dashed lines with the same color for comparison.

S4 and Figure S5) of the acid, the catalytic wave appears better defined when AcOH was added as a proton source. The addition of trifluoroacetic acid (TFA, pK_a = 6)^[38] as proton source leads to a different behavior. An irreversible reduction peak appears at −0.16 V (Figure 4c, Figure S6). The identical presence of this peak, both in the absence and presence of oxygen, indicates

protonation of the **CuL** complex (Figure S7). In the presence of TFA, the same ORR signal is observed both in the presence and absence of **CuL** (Figure 4c), suggesting that **CuL** does not act as a catalyst for the ORR in the presence of TFA. Additional UV-visible measurements carried out on **CuL** in the absence and presence of TFA reveal identical features. These data confirm that the structure of the complex does not change in the presence of TFA so that the protonation only occurs following the reduction process (Figure S8).

As specific for electrochemical processes, the energy-efficiency of the ORR depends on the driving force required for the reaction to proceed at a significant rate. This driving force is quantified as the overpotential, defined as the difference between the applied potential to drive the ORR and the thermodynamic equilibrium potential of the ORR. The standard potential of ORR to form H_2O in DMF and in the presence of an acid as proton source (denoted as HA), expressed by equation (1) according to previous calculations,^[18, 39] was reported in Table 1 for the conditions considered in this study.

$$E_{\text{O}_2/\text{H}_2\text{O,HA,DMF}}^0 = 0.799 - \frac{RT \ln 10}{F} pK_{\text{a,HA,DMF}} \quad (1)$$

An accurate benchmarking of the performances of the homogeneous ORR catalysts should involve the construction of a *catalytic Tafel plot*.^[40-41] However, the required methodology to collect accurate kinetic data for such $4\text{e}^-/4\text{H}^+$ O_2 reduction process to H_2O involving two distinct reactants is still incomplete. Instead, the overpotential requirement (denoted ΔE^{ORR} , Table 1) to drive ORR can provide the basis for a relevant analysis of the homogeneous ORR catalysts. ΔE^{ORR} is expressed as the difference between the standard potential of ORR ($E_{\text{O}_2/\text{H}_2\text{O,HA,DMF}}^0$) and the half-wave potential of the ORR catalytic wave (denoted $E_{\text{cat}/2}^{\text{ORR}}$, equation (2)) under the conditions used for the measurement.^[18, 40]

$$\Delta E^{\text{ORR}} = E_{\text{O}_2/\text{H}_2\text{O,HA,DMF}}^0 - E_{\text{cat}/2}^{\text{ORR}} \quad (2)$$

Table 1 summarizes the experimental ΔE^{ORR} values for **CuL** in DMF as function of the strength (pK_{a}) of acids.

Table 1. pK_{a} of different acids and main parameters for the ORR with **CuL** in DMF

| Acid | $pK_{\text{a,HA}}$ | $E_{\text{O}_2/\text{H}_2\text{O,HA,DMF}}^0$ (V vs NHE) | $E_{\text{cat}/2}^{\text{ORR}}$ (V vs NHE) | ΔE^{ORR} (V vs NHE) |
|------|----------------------|--|---|---------------------------------------|
| PhOH | 18.8 ^[37] | -0.329 | -0.495 | 0.166 |
| AcOH | 13.3 ^[38] | -0.010 | -0.480 | 0.490 |

Rotating ring-disk electrode (RRDE) voltammograms were recorded in DMF with **CuL** in solution for quantifying the production of H_2O_2 in the presence of PhOH and AcOH under electrochemical conditions and estimating **CuL** selectivity for $2\text{e}^-/2\text{H}^+$ vs $4\text{e}^-/4\text{H}^+$ O_2 reduction. The potential at the GC disk was scanned through the catalytic region (from -0.2 V to -0.6 V vs NHE) and the potential at the Pt ring was fixed at 1.07 V vs NHE in order to detect the oxidation of the ORR-generated hydrogen peroxide. Figure 5 presents typical RRDE voltammograms showing the ring and disk currents obtained from ORR. ORR catalytic currents were observed at the disk, in

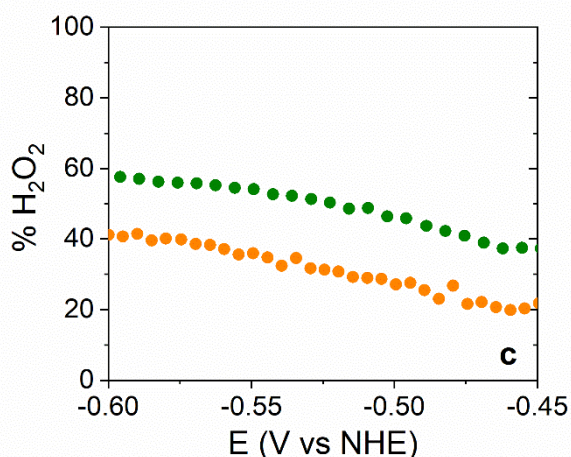
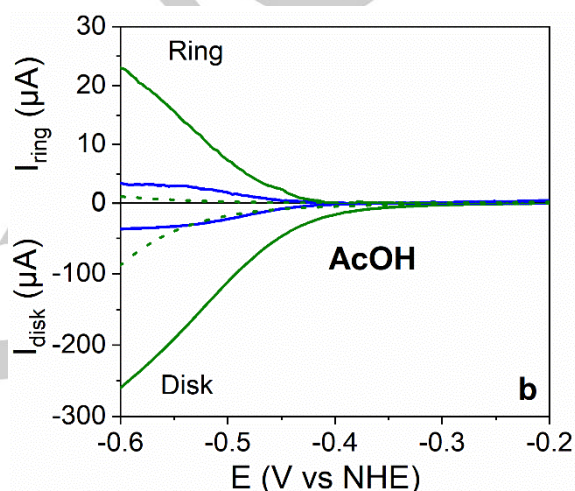
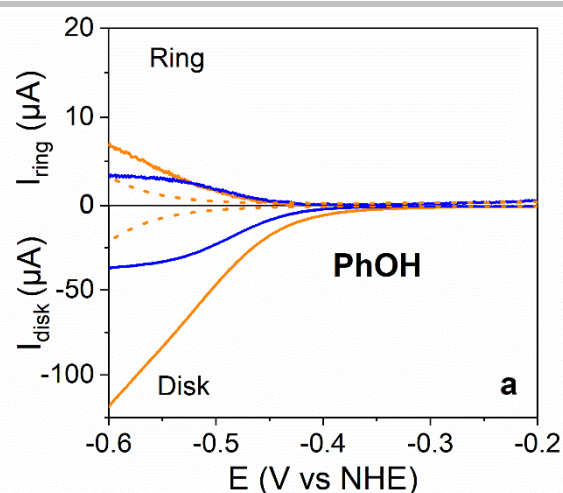


Figure 5. (a, b). Rotating ring-disk electrodes (RRDE) voltammograms under O_2 -saturated atmosphere in DMF (0.1 M $^{\text{nBu}_4\text{NPF}_6}$) on GC electrode (\varnothing 5 mm), scan rate $10 \text{ mV}\cdot\text{s}^{-1}$, 500 rpm, ring current recorded with Pt ring held at 1.07 V vs NHE. All blue curves are for **CuL** (1 mM), a). **CuL** (1 mM) + PhOH (50 mM, orange trace) and b). **CuL** (1 mM) + AcOH (50 mM, green trace). The RRDE voltammograms of acids in the absence of **CuL** are shown as dashed line for comparison. In the orange and green plain curves, I_{ring} has been corrected by subtracting of the value measured without acid. (c). The RRDE-determined % of produced H_2O_2 for reduction of one molecule of O_2 vs applied potential for the two different acids (same color code).

accordance with previously discussed CVs measurements (Figure 4). The ring currents, which follow the shape of the disk

currents (Figure 5), can be attributed to the oxidation of the species generated in the reduction processes at the disk, which can be either reduced forms of **CuL** and H_2O_2 . In the control experiments performed in the presence of **CuL** without acid, the ring currents correspond only to the reoxidation of reduced forms of **CuL**. Thus, for a proper evaluation of the ORR process, I_{ring} measured in the presence of acid has been corrected by subtracting I_{ring} measured without acid. Another series of control experiments was performed in the absence of **CuL** (Figure 5, dashed curves) and revealed that the O_2 -reduction process occurring directly at the GC disk is only observed in the presence of acids and at more negative potentials. Figure 5c shows the corresponding Faradaic efficiencies for H_2O_2 production mediated by **CuL** in DMF in the presence of acids in the explored potential window, obtained by application of equation (3) at 500 rpm. The Faradaic efficiencies for H_2O_2 production vary from 20 % to 41 % (PhOH) or from 37 % to 59 % (AcOH) in the potential window from -0.45 V to -0.6 V vs NHE (Figure 5c). Data are summarized in Table S4. Nevertheless, **CuL** catalyzes the O_2 reduction by combined $4\text{e}^-/4\text{H}^+$ and $2\text{e}^-/2\text{H}^+$ processes in the presence of PhOH or AcOH. A slight improved selectivity of **CuL** toward H_2O production was observed with the weakest acid, PhOH, which remains lower than the one observed for other mononuclear^[30] or binuclear^[32] copper complexes evaluated under similar RRDE experiments, in aqueous solutions.

The ORR selectivity for H_2O production has been shown to depend on the thermodynamic standard potential, being controlled by the pK_a of the proton donor.^[18] Nocera and co-workers indeed showed for several Co- and Fe-based molecular catalysts a correlation between the selectivity of catalyst for H_2O production and the overpotential requirement for ORR. They showed that the ORR pathway to H_2O production is favoured in the presence of stronger acid where there is a higher overpotential requirement for ORR. As a consequence, the ORR selectivity for H_2O production was also found better for the same overpotential requirement when DMF is used as a solvent in DMF. Our data are plotted in Figure 6, therefore modified from ref.^[18] When PhOH is used as the proton source, **CuL** behaves as other catalysts tested in DMF and displays selectivity closes to the one reported for the dicobalt $[\text{Co}_2(\text{OH})_2\text{DPEN}(\mu-1,3\text{-OC}(\text{NH})\text{CH}_3)]^{3+}$ (DPEN = dipyriddyethane naphthyridine) complex. This data point (**CuL**/PhOH, 73 % H_2O for ΔE^{ORR} of 0.166 V) confirms the trend already observed by Nocera and co-workers. However, the selectivity measured for **CuL** when AcOH is used as proton source, does not follow the same correlation. With the same catalyst and by employing a stronger acid, a lower ORR selectivity for H_2O was achieved for a higher overpotential requirement (59 % H_2O for ΔE^{ORR} of 0.490 V). This behaviour, together with the point measured for iron tetraphenylporphyrin in Figure 6,^[18] indicates that the overpotential requirement cannot be used as the only descriptor of the selectivity of ORR. Actually, our results are consistent with a recent study on a series of Co-based molecular catalysts.^[15] This indicated that selectivity depends on the relative position of the redox potential of the catalyst (CoIII/II in that case) versus the potential of the $\text{O}_2/\text{H}_2\text{O}_2$ couple, with stronger acids favoring H_2O_2 formation while lowering the overpotential for ORR. Of note, free-energy linear correlations (scaling relationships) observed for various catalysts indicate that the same mechanism (or at least the same rate determining step) prevails within the whole series. On the reverse, the fact that few data points measured in DMF are offline the correlations in Figure 6

indicates that these catalysts likely follow a distinct route for ORR, calling for further mechanistic studies.

Despite of a lower selectivity of O_2 reduction to H_2O catalysed by the **CuL** complex than by a binuclear copper complex^[32] or another mononuclear Cu-tmpa complex^[30] evaluated under similar RRDE experiments, new insights on the evaluation of homogeneous ORR with Cu complexes have been gathered.

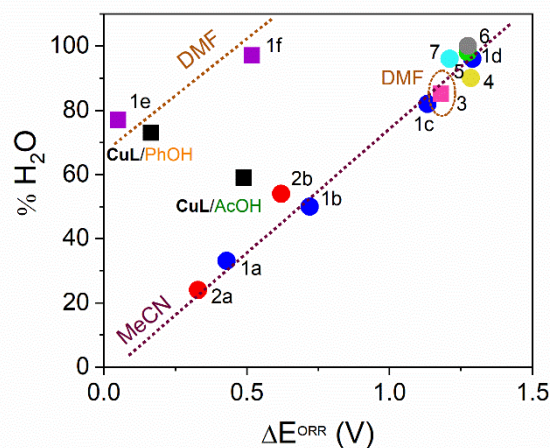


Figure 6. Faradaic efficiency for H_2O production vs ΔE^{ORR} for **CuL** (black) in the presence of PhOH, AcOH and TFA in DMF (0.1 M $^n\text{Bu}_4\text{NPF}_6$) and comparison with other catalysts: (1) $[\text{Co}_2(\text{OH})_2\text{DPEN}(\mu-1,3\text{-OC}(\text{NH})\text{CH}_3)]^{3+}$ (DPEN = dipyriddyethane naphthyridine) in MeCN (blue) with (1a) PhOH, (1b) AcOH, (1c) ClCH_2COOH , (1d) TFA;^[18] (1) in DMF with (purple) (1e) AcOH, (1f) TFA; (2) $[\text{Co}_2(\text{OH})_2\text{DPEN}(\mu-1,3\text{-OAc})]^{3+}$ in MeCN (red) with (2a) PhOH, (2b) AcOH;^[18] (3) Fe tetraphenylporphyrin in DMF with HClO_4 (pink);^[42] (4) Fe meso-tetra(2-carboxyphenyl)porphyrin in MeCN with $(\text{HDMF})^+$ (yellow);^[43] (5) Fe meso-tetra(4-carboxyphenyl)porphyrin in MeCN with $(\text{HDMF})^+$ (green).^[43] (6) $\text{Co}^{\text{III}}_2(\text{trpy})_2(\mu\text{-bpp})(\mu-1,2\text{-O}_2)]^{3+}$ (bpp = bis-(pyridyl)-pyrazolate, trpy = terpyridine) in MeCN with TFA (gray);^[44] (7) $[\text{Fe}^{\text{II}}_2(\text{LS})(\text{LSH})]$ ($\text{LS}^{2-} = 2,2'-(2,2'$ -bipyridine-6,6'-diyl)bis-(1,1-diphenylethanethiolate) in MeCN with lutidinium.^[14] Data measured in CH_3CN are indicated as dots while data obtained in DMF are shown as squares. Dotted lines are just guides for the eye to indicate the free energy linear correlations in both solvents [Adapted with permission from ref. 18 Copyright (2016) American Chemical Society].

Conclusion

Despite their relevance as bioinspired O_2 -reduction catalysts, quite few studies are available for homogeneous copper-based molecular complex as ORR catalysts. We provide here one example of such an active mononuclear copper catalyst, copper(II) thiosemicarbazone complex (**CuL**) that catalyzes the O_2 reduction by combined $4\text{e}^-/4\text{H}^+$ and $2\text{e}^-/2\text{H}^+$ processes in the presence of PhOH or AcOH. A better selectivity for the $4\text{e}^-/4\text{H}^+$ reduction of O_2 to H_2O can be attained with the PhOH as proton source. Our data in the presence of PhOH partially confirm the previously established free energy linear correlation between selectivity and overpotential requirement. Interestingly, in the presence of AcOH, a stronger acid than PhOH, the correlation was not observed, likely indicating for a change in the catalytic ORR mechanism. Future work will aim at understanding the catalytic mechanism and establishing structure-function relationships able to rationalize such a design.

Experimental Section

Materials and Reagents

Synthetic starting precursors, solvents, tetrabutylammonium hexafluorophosphate ($n\text{Bu}_4\text{NPF}_6$) supporting electrolyte and all other chemicals agents were purchased from Sigma Aldrich. All chemical reagents were of analytical grade and were used as received without further purification. The synthesis of the H_2L ligand was performed according to previously described procedures.^[33] Oxygen gas (Air Products ultrapure quality) was 99.995 % purity.

Physical and chemical characterization

Elemental analysis was performed on a Thermo Finnigan EA 1112 instrument. The results were validated by at least two sets of measurements. IR spectra were recorded with a Bruker TENSOR 27 spectrometer equipped with a single-reflection DuraSamplIR diamond. Electronic absorption spectra were recorded with Hitachi U3310 and Perkin Elmer's LAMBDA 25 UV-Vis systems instruments controlled with UV Solutions or UV WinLab utilities, respectively.

Synthesis of CuL complex

A solution of $\text{Cu}(\text{NO}_3)_2 \cdot 4\text{H}_2\text{O}$ (0.058g, 0.225 mmol) in methanol (2 mL) was added dropwise to a suspension of the 4-{bis(4-(p-methoxyphenyl)-thiosemicarbazone)-2,3-butane (H_2L) ligand (0.1 g, 0.225 mmol) in methanol (5 mL). The mixture was stirred at reflux for 2 h. The resulting red precipitate was collected by filtration, washed with methanol and dried in the air (80 mg, yield: 70 %). elemental analysis calc. (%) for $\text{C}_{20}\text{H}_{24}\text{N}_6\text{O}_2\text{S}_2\text{Cu}$ (506.11 $\text{g}\cdot\text{mol}^{-1}$): C 47.43, H 4.34, N 16.58, S 12.64; found: C 47.36, H 4.07, N 16.59, S 12.27. FT-IR (ATR): $\bar{\nu}$ = 3292 (N-H), 1598 (C=N imine), 1508 (N-C), 1240 and 1029 (O-C), 1176 and 821 (C-S) cm^{-1} .

Crystallographic characterization

Diffraction data were collected using an Oxford Diffraction XCallibur S Kappa area detector four-circle diffractometer (Mo-K α radiation λ = 0.71073 Å, graphite monochromator), controlled by the Oxford Diffraction CrysAlis CCD software. Unique intensities with $I > 10\sigma(I)$ detected on all frames using the Oxford Diffraction RED were used to refine the values of the cell parameters. The substantial redundancy in data allows analytical absorption corrections to be applied using crystal shape determination for **CuL** complex. The space group was determined from systematic absences, and it was confirmed by the successful resolution of the structure. The structure was solved by charge flipping method using ShelXS in Olex1.2 environment. All the atoms were found by difference Fourier syntheses. All non-hydrogen atoms were anisotropically refined on F2 using ShelXL program. Hydrogen atoms were fixed in ideal positions for complex and found by fourier transformation and refined isotropically.

Crystals of **CuL** suitable for X-ray diffraction analysis were obtained by slow evaporation of a THF solution. The **CuL** complex crystallizes in the monoclinic system with $\text{P}2_1/n$ space group (Table S5). The crystal consists of a neutral mononuclear [**CuL**] unit and THF as solvent molecules in 1:1 ratio. The asymmetric unit consists of a neutral mononuclear **CuL** unit and 1 THF solvent molecule in general positions. Crystallographic data for [**CuL**].THF (CCDC-1548059) can be obtained free of charge from The Cambridge Crystallographic Data Centre via: www.ccdc.cam.ac.uk/data_request/cif.

Electrochemical measurements

Electrochemical measurements were carried out with a SP-300 Bio-Logic bipotentiostat in a conventional three-electrode cell, using a stationary glassy carbon (GC) disk (ϕ 1.6 mm) working electrode, a platinum wire

as counter electrode and a Ag/AgCl, KCl (3 M) (denoted below Ag/AgCl) as the reference electrode. This Ag/AgCl reference electrode was calibrated with the internal $\text{Fc}^{+/0}$ reference system after each experiment, which was found at +0.55 V vs Ag/AgCl. The $\text{Fc}^{+/0}$ couple (E^0 for $\text{Fc}^{+/0}$ = 0.57 V vs NHE, taking into account interliquid junction potential)^[45-47] was further used to convert potentials vs. NHE. The working electrode was polished before each measurement on a MD-Nap polishing pad with a 1 μm monocrystalline diamond paste, rinsed with ethanol and dried under air.

Cyclic voltammograms were recorded at a scan rate of 100 $\text{mV}\cdot\text{s}^{-1}$ in *N,N*-dimethylformamide (DMF) with $n\text{Bu}_4\text{NPF}_6$ (0.1 M) supporting electrolyte at room temperature, under argon or oxygen atmosphere.

The 1M solutions of phenol (PhOH), acetic acid (AcOH) and trifluoroacetic acid (TFA) in DMF were added with a microsyringe.

Spectroelectrochemical experiments were performed in Thin Layer Quartz Glass Spectroelectrochemical cell Kit (Bio-Logic) using a platinum grid as working electrode, a platinum wire as counter electrode and a Ag/AgCl reference electrode.

The catalytic activity of the **CuL** complex towards the ORR was investigated using the rotating ring-disk electrode (RRDE) technique. Pine RRDE setup with a glassy carbon disk (ϕ 5 mm, 0.196 cm^2) and a Pt ring (0.110 cm^2) was used as working electrode. RRDE experiments were carried out under O_2 -saturated solution. Polarization curves were recorded at 10 $\text{mV}\cdot\text{s}^{-1}$, with a rotation speed of 500 rpm. The potential of the Pt ring was set at 1.07 V vs NHE. The faradaic efficiency for H_2O_2 production as a function of potential applied at the disk is obtained according with equation (3).^[48]

$$\% \text{H}_2\text{O}_2 = \frac{2I_r(E)/N}{I_d(E) + I_r(E)/N} \times 100 \quad (3)$$

where $I_r(E)$ and $I_d(E)$ are the absolute values of ring and disk current at potential E and N is the collection efficiency of the electrode. The value of N was determined to be 0.221 using the one-electron $[\text{Fe}(\text{CN})_6]^{3-/4-}$ redox couple.

Theoretical calculations

Density-functional theory (DFT) calculations were performed with the ORCA program package.^[49] Full geometry optimizations were undertaken for all complexes using the GGA functional BP86^[50-52] in combination with the TZV/P basis^[53] set for all atoms, and by taking advantage of the resolution of the identity (RI) approximation in the Split-RI-J variant^[54] with the appropriate Coulomb fitting sets.^[55] Increased integration grids (Grid4 in ORCA convention) and tight SCF convergence criteria were used. Electronic structures and Molecular Orbital diagrams were obtained from single-point calculations using the hybrid functional B3LYP^[56-57] together with the TZV/P basis set. Increased integration grids (Grid4 and GridX4 in ORCA convention) and tight SCF convergence criteria were used in the calculations. For according to the experimental conditions solvent effects were accounted and we used the DMF solvent (ϵ = 37) within the framework of the conductor-like screening (COSMO) dielectric continuum approach.^[58] The relative energies were computed from the gas-phase optimized structures as a sum of electronic energy, solvation and thermal corrections to the free energy. Redox potentials were evaluated by employing a Born-Haber thermodynamic cycle following the same procedure that was previously employed for the characterization of our cobalt analogue (see Supplementary Information for details). Spin density plots as well as molecular orbitals were generated using the orca plot utility program and were visualized with the Chemcraft program.^[59]

Acknowledgements

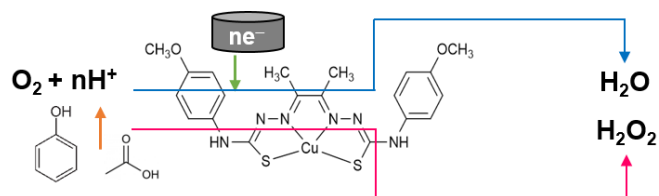
This work was supported by the Agence Nationale de la Recherche (Labex ARCANE, CBH-EUR-GS, ANR-17-EURE-0003).

Keywords: oxygen reduction reaction (ORR) • homogeneous catalysis • ORR selectivity • overpotential requirement • scaling relationships

References

- [1] X. Huang and J. T. Groves, *Chem. Rev.* **2018**, *118*, 2491-2553.
- [2] I. Katsounaros, S. Cherevko, A. R. Zeradjanin and K. J. J. Mayrhofer, *Angew. Chem. Int. Ed.* **2014**, *53*, 102-121.
- [3] K. Krumova and G. Cosa in *Chapter 1 Overview of Reactive Oxygen Species, Vol. 1* The Royal Society of Chemistry, **2016**, pp. 1-21.
- [4] S. Ferguson-Miller and G. T. Babcock, *Chem. Rev.* **1996**, *96*, 2889-2908.
- [5] M. M. Pereira, M. Santana and M. Teixeira, *Biochim. Biophys. Acta* **2001**, *1505*, 185-208.
- [6] E. Vayner, H. Schweiger and A. B. Anderson, *J. Electroanal. Chem.* **2007**, *607*, 90-100.
- [7] E. I. Solomon, U. M. Sundaram and T. E. Machonkin, *Chem. Rev.* **1996**, *96*, 2563-2606.
- [8] B. Zhang and L. Sun, *Chem. Soc. Rev.* **2019**, *48*, 2216-2264.
- [9] M. L. Pegis, C. F. Wise, D. J. Martin and J. M. Mayer, *Chem. Rev.* **2018**, *118*, 2340-2391.
- [10] S. Dey, B. Mondal, S. Chatterjee, A. Rana, S. Amanullah and A. Dey, *Nat. Rev. Chem.* **2017**, *1*, 0098.
- [11] C. W. Machan, *ACS Catal.* **2020**, *10*, 2640-2655.
- [12] S. Fukuzumi, Y.-M. Lee and W. Nam, *ChemCatChem* **2018**, *10*, 9-28.
- [13] M. L. Pegis, B. A. McKeown, N. Kumar, K. Lang, D. J. Wasylenko, X. P. Zhang, S. Raagei and J. M. Mayer, *ACS Cent. Sci.* **2016**, *2*, 850-856.
- [14] L. Wang, M. Gennari, F. G. Cantú Reinhard, J. Gutiérrez, A. Morozan, C. Philouze, S. Demeshko, V. Artero, F. Meyer, S. P. de Visser and C. Duboc, *J. Am. Chem. Soc.* **2019**, *141*, 8244-8253.
- [15] Y.-H. Wang, P. E. Schneider, Z. K. Goldsmith, B. Mondal, S. Hammes-Schiffer and S. S. Stahl, *ACS Cent. Sci.* **2019**, *5*, 1024-1034.
- [16] R. Jasinski, *Nature* **1964**, *201*, 1212-1213.
- [17] M. L. Pegis, J. A. S. Roberts, D. J. Wasylenko, E. A. Mader, A. M. Appel and J. M. Mayer, *Inorg. Chem.* **2015**, *54*, 11883-11888.
- [18] G. Passard, A. M. Ullman, C. N. Brodsky and D. G. Nocera, *J. Am. Chem. Soc.* **2016**, *138*, 2925-2928.
- [19] L. M. Mirica, X. Ottenwaelder and T. D. P. Stack, *Chem. Rev.* **2004**, *104*, 1013-1046.
- [20] M. A. Thorseth, C. E. Tornow, E. C. M. Tse and A. A. Gewirth, *Coord. Chem. Rev.* **2013**, *257*, 130-139.
- [21] C. E. Elwell, N. L. Gagnon, B. D. Neisen, D. Dhar, A. D. Spaeth, G. M. Yee and W. B. Tolman, *Chem. Rev.* **2017**, *117*, 2059-2107.
- [22] S. M. Adam, G. B. Wijeratne, P. J. Rogler, D. E. Diaz, D. A. Quist, J. J. Liu and K. D. Karlin, *Chem. Rev.* **2018**, *118*, 10840-11022.
- [23] J. Zhang and F. C. Anson, *J. Electroanal. Chem.* **1992**, *341*, 323-341.
- [24] M. S. Thorum, J. Yadav and A. A. Gewirth, *Angew. Chem. Int. Ed.* **2009**, *48*, 165-167.
- [25] C. C. L. McCrory, A. Devadoss, X. Ottenwaelder, R. D. Lowe, T. D. P. Stack and C. E. D. Chidsey, *J. Am. Chem. Soc.* **2011**, *133*, 3696-3699.
- [26] S. Gentil, D. Serre, C. Philouze, M. Holzinger, F. Thomas and A. Le Goff, *Angew. Chem. Int. Ed.* **2016**, *55*, 2517-2520.
- [27] S. Gentil, J. K. Molloy, M. Carrière, A. Hobballah, A. Dutta, S. Cosnier, W. J. Shaw, G. Gellon, C. Belle, V. Artero, F. Thomas and A. Le Goff, *Joule* **2019**, *3*, 2020-2029.
- [28] S. Fukuzumi, H. Kotani, H. R. Lucas, K. Doi, T. Suenobu, R. L. Peterson and K. D. Karlin, *J. Am. Chem. Soc.* **2010**, *132*, 6874-6875.
- [29] S. Kakuda, R. L. Peterson, K. Ohkubo, K. D. Karlin and S. Fukuzumi, *J. Am. Chem. Soc.* **2013**, *135*, 6513-6522.
- [30] M. Langerman and D. G. H. Hetterscheid, *Angew. Chem. Int. Ed.* **2019**, *58*, 12974-12978.
- [31] S. Fukuzumi, L. Tahsini, Y.-M. Lee, K. Ohkubo, W. Nam and K. D. Karlin, *J. Am. Chem. Soc.* **2012**, *134*, 7025-7035.
- [32] C. Liu, H. Lei, Z. Zhang, F. Chen and R. Cao, *Chem. Commun.* **2017**, *53*, 3189-3192.
- [33] T. Straistari, J. Fize, S. Shova, M. Reglier, V. Artero and M. Orto, *ChemCatChem* **2017**, *9*, 2262-2268.
- [34] T. Straistari, R. Hardré, J. Fize, S. Shova, M. Giorgi, M. Réglier, V. Artero and M. Orto, *Chem. Eur. J.* **2018**, *24*, 8779-8786.
- [35] A. A. Abou-Hussen, N. M. El-Metwally, E. M. Saad and A. A. El-Asmy, *J. Coord. Chem.* **2005**, *58*, 1735-1749.
- [36] M. B. Ferrari, G. G. Fava, C. Pelizzi, G. Pelosi and P. Tarasconi, *Inorg. Chim. Acta* **1998**, *269*, 297-301.
- [37] K. Izutsu, *Acid-Base Dissociation Constants in Dipolar Aprotic Solvents*, Wiley-Blackwell, **1990**, p. 176.
- [38] C. P. Andrieux, J. Gamby, P. Hapiot and J.-M. Savéant, *J. Am. Chem. Soc.* **2003**, *125*, 10119-10124.
- [39] C. Costentin, T. R. Porter and J.-M. Savéant, *J. Am. Chem. Soc.* **2016**, *138*, 5615-5622.
- [40] C. Costentin, S. Drouet, M. Robert and J.-M. Savéant, *J. Am. Chem. Soc.* **2012**, *134*, 11235-11242.
- [41] V. Artero and J.-M. Saveant, *Energy Environ. Sci.* **2014**, *7*, 3808-3814.
- [42] D. J. Wasylenko, C. Rodriguez, M. L. Pegis and J. M. Mayer, *J. Am. Chem. Soc.* **2014**, *136*, 12544-12547.
- [43] C. T. Carver, B. D. Matson and J. M. Mayer, *J. Am. Chem. Soc.* **2012**, *134*, 5444-5447.
- [44] S. Fukuzumi, S. Mandal, K. Mase, K. Ohkubo, H. Park, J. Benet-Buchholz, W. Nam and A. Llobet, *J. Am. Chem. Soc.* **2012**, *134*, 9906-9909.
- [45] C. Costentin, S. Drouet, M. Robert and J. M. Saveant, *Science* **2012**, *338*, 90-94.
- [46] T. N. Huan, E. S. Andreiadis, J. Heidkamp, P. Simon, E. Derat, S. Cobo, G. Royal, A. Bergmann, P. Strasser, H. Dau, V. Artero and M. Fontecave, *J. Mater. Chem. A* **2015**, *3*, 3901-3907.
- [47] T. N. Huan, P. Simon, G. Rousse, I. Genois, V. Artero and M. Fontecave, *Chem. Sci.* **2017**, *8*, 742-747.
- [48] Z. Jia, G. Yin and J. Zhang in *Rotating ring-disk electrode method*, Vol. Elsevier B. V., **2014**, pp. 199-228.
- [49] F. Neese, *WIREs Comput. Mol. Sci.* **2012**, *2*, 73-78.
- [50] J. P. Perdew, *Phys. Rev. B* **1986**, *33*, 8822-8824.
- [51] J. P. Perdew, *Physical Review B* **1986**, *34*, 7406-7406.
- [52] A. D. Becke, *Phys. Rev. A* **1988**, *38*, 3098-3100.
- [53] A. Schafer, C. Huber and R. Ahlrichs, *J. Chem. Phys.* **1994**, *100*, 5829-5835.
- [54] F. Neese, *J. Comput. Chem.* **2003**, *24*, 1740-1747.
- [55] F. Weigend, *Phys. Chem. Chem. Phys.* **2006**, *8*, 1057-1065.
- [56] A. D. Becke, *J. Chem. Phys.* **1993**, *98*, 1372-1377.
- [57] C. Lee, W. Yang and R. G. Parr, *Physical Review B* **1988**, *37*, 785-789.
- [58] A. Klamt and G. Schuurmann, *J. Chem. Soc., Perkin Trans. 2* **1993**, 799-805.
- [59] Chemcraft in *Chemcraft*, <http://chemcraftprog.com>.

Entry for the Table of Contents



The mononuclear, copper(II) thiosemicarbazone complex (**CuL**) catalyzes the homogeneous oxygen reduction reaction (ORR) via a combined 4H⁺/4e⁻ and 2H⁺/2e⁻ processes in the presence of various organic acids as proton sources.